Thermally Induced Persistent Covalent-Organic Frameworks Radicals

Qianfeng Gu, Xiangqian Lu, Cailing Chen, Renjie Hu, Xin Wang, Guohan Sun, Fangyuan KANG, Jinglun Yang, Xiang Wang, Jinghang Wu, Yang Yang Li, Yung-Kang Peng, Wei Qin,* Yu Han,* Xiaogang Liu,* and Qichun Zhang*

Read Online

ACCESS | Metrics & More | Article Recommendations | Supporting Information

ABSTRACT: Persistent covalent-organic framework (COF) radicals hold important applications in magnetics and spintronics; however, their facile synthesis remains a daunting challenge. Here, three *p*-phenylenediacetonitrile-based COFs (named CityU-4, CityU-5, and CityU-6) were synthesized. Upon heat treatment (250 °C for CityU-4 and CityU-5 or 220 °C for CityU-6), these frameworks were brought into their persistent radical forms (no obvious changes after at least one year), together with several observable factors, including color changes, red-shifted absorption, the appearance of electron spin resonance (ESR) signals, and detectable magnetic susceptibility. The theoretical simulation suggests that after heat treatment, lower total energy and nonzero spin density are two main factors to guarantee persistent COFs radicals and polarized spin distributions. This work provides an efficient method for the preparation of persistent COF radicals with promising potentials.

KEYWORDS: covalent organic frameworks, COF radicals, thermally induced radicals, spin polarization, magnetic susceptibility
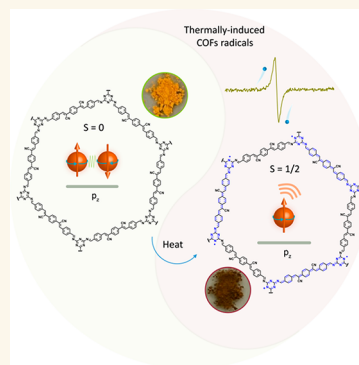
INTRODUCTION

Organic radicals with narrow HOMO−LUMO energy gaps, low-lying doubly excited states and redox amphotericity have wide applications in organic electronics, photonics and spintronics.[1−5] However, owing to their open-shell and subvalent features as well as their intrinsic thermodynamic and kinetic instability, organic radicals normally have high reactivity, leading to the formation of covalent bonds through dimerization, disproportionation, or hydrogen abstraction. To address these issues and obtain persistent organic radicals with net spin, bulky substituents are widely adopted to increase the kinetic stability and prevent dimerization or oxidization reactions. Another approach to enhance the radical stability is to improve the delocalization of the unpaired electrons through constructing large conjugated π system with extensively delocalized π-electrons.[2,6,7] However, it is still very challenging to develop a simple method for the preparation of stable organic radicals under ambient conditions.

As an important material, π-conjugated covalent-organic frameworks (COFs) with delocalized electrons could be promising candidates to produce stable organic radicals.[2] In fact, owing to the programmability and tunability of their composition, structure, and porosity, COFs have been demonstrated as effective core components for various applications, including gas adsorption, catalysis, rechargeable batteries, and external-stimulus-responsive devices.[8−21] To further expand their functionality, incorporation of radicals into COFs to form radicals arrays could offer an additional dimension for manipulating electron spins, thereby endowing COFs with unique electronic/magnetic properties for wide applications in organic semiconducting devices such as spin valve, magnetics, and thermoelectrics.[5,22−28] Introducing radicals into COFs can be achieved through several strategies, including direct radical implantation, chemical treatment, and irradiation.[11,23,29−33] However, COF radicals prepared by these methods usually require either a complicated framework design, a tedious synthesis, or a harsh treatment (redox or radiation), resulting in unstable radicals and severely limiting their applications. To address this issue, it is highly desirable to develop a facile method for the preparation of persistent neutral COF radicals, given the oxygen/moisture-sensitive nature of organic radical cations/anions.[34,35]
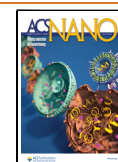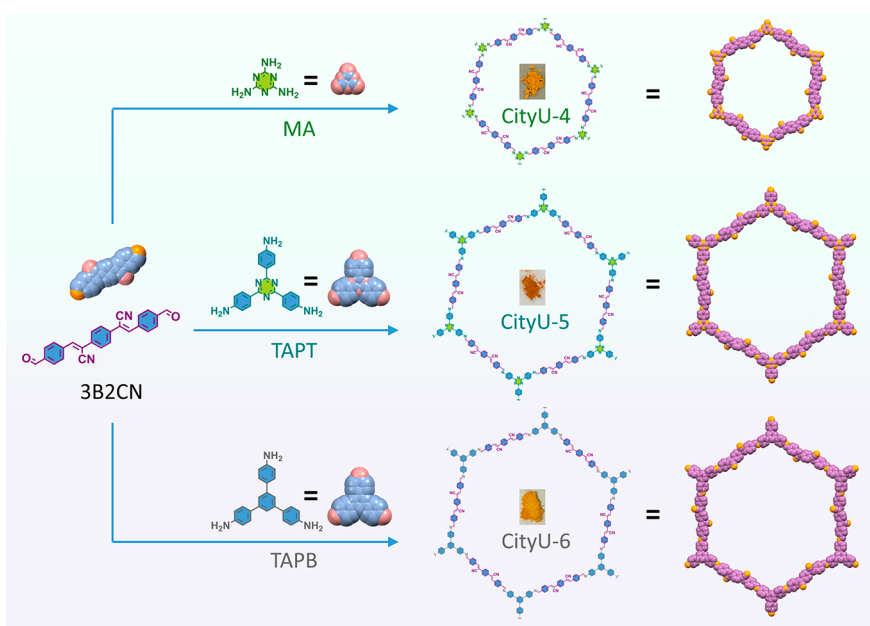
Figure 1. Synthetic route to three crystalline COFs (CityU-4, CityU-5, and CityU-6). The insets are photos of the as-obtained COF powders.

Herein, taking advantage of the effect of temperature on structural conformation,[36,37] the modulated electronic structures with perturbed resonance forms can be realized through thermal treatment to generate persistent COF radicals.[5,38−41] Besides, covalent triazine frameworks (CTFs) typically with high porosity and good thermal and chemical stability were judiciously designed with arylamine based COFs as comparison. In a typical procedure, we synthesized three crystalline COFs (named as **CityU-4**, **CityU-5**, and **CityU-6**) containing *p*-phenylenediacetonitrile building units as electronic isolation units for the stabilization of radicals.[4] Upon heating these COFs were heated to specific temperatures (250 °C for **CityU-4** and **CityU-5** or 220 °C for **CityU-6**), we observed distinct changes, indicating the formation of radicals. These changes include the alterations in color, red-shifted absorbance, the appearance of electron spin resonance (ESR) signals, and detectable magnetic susceptibility. The radical nature of the COFs remained stable for at least one year without any observable change. Our theoretical studies through density functional theory (DFT) simulations further reveal that the generation of stable COFs radicals with spin polarization is associated with lower total energy and the presence of electron delocalization, leading to nonzero net spin density. This work provides a simple and feasible preparation process for producing persistent COFs radicals without special apparatuses, which is suitable for mass production and promotion.

RESULTS AND DISCUSSION

Synthesis and Characterizations of Pristine COFs. Three *p*-phenylenediacetonitrile-based isoreticular COFs (**CityU-4**, **CityU-5**, and **CityU-6**) were prepared through a polycondensation reaction between 3B2CN (short for (2Z,2′Z)-2,2′-(1,4-phenylene)bis(3-(4-formylphenyl)-acrylonitrile, Figure S1) and three amines, including melamine (MA), tris(4-aminophenyl)triazine (TAPT), and 1,3,5-tris(4-aminophenyl)benzene (TAPB) in mixed solvents of 1,4-dioxane, aniline, and 6 M acetic acid (HOAc) (25:3:5 in v/v/v) at 150 °C for 3 days (Figure 1), with aniline introduced to control the growth of crystalline COFs.[42] After Soxhlet

extraction, these three COFs were activated under a vacuum at 150 °C to remove the probable guest molecules (monomers) before further characterization and heat treatment.

The chemical structures of **CityU-4**, **CityU-5**, and **CityU-6** were identified through Fourier-transform infrared (FTIR) spectroscopy (Figure S2), where the enlarged FTIR spectra were provided for better comparison (Figures S3 and S4). After condensation, the characteristic peaks of aldehyde (∼1690 cm^{-1}) and amino groups (3470, 3320, and 3200 cm^{-1}) disappeared and a new peak at 1616 cm^{-1}, belonging to a typical stretching imine bond, was observed in products. Moreover, the characteristic peaks of the cyano group ($v_{C\equiv N}$, ∼2220 cm^{-1}), triazine group (1633, 1579, and 1500 cm^{-1}), and benzene ring (1614, 1506, and 1465 cm^{-1}) from precursors were still found in three as-prepared products, suggesting the successful condensation reaction with the formtion of pivotal C=N linkages of three COFs.

The crystallinity of **CityU-4**, **CityU-5**, and **CityU-6** was confirmed by small-angle powder X-ray diffraction (PXRD) analysis, where several diffraction peaks for **CityU-4** (Figure 2a, 2θ = 2.9°, 11.6°, 14.5°, 15.2°, 17.4°, 23.8°, 26.2°, and 27.7°, corresponding to (100), (400), (500), (420), (600), (810), (001), and (830) facets), **CityU-5** (Figure 2b, 2θ = 2.8°, 11.5°, 14.4°, 15.1°, 17.3°, 23.7°, and 27.7°, corresponding to (100), (400), (500), (420), (600), (810), and (830) facets), and **CityU-6** (Figure 2c, 2θ = 2.5°, 11.3°, 15.1°, 17.3°, 19.3°, 20.1°, 23.6°, and 27.7°, corresponding to (100), (400), (420), (600), (810), and (830) facets) were observed. The diffraction signals are not from the monomers owing to the dramatic difference between the signals of COFs and corresponding monomers (Figure S5). Their structures were further studied through structural simulations and Pawley refinement by considering the geometry and connectivity of their precursors.[35,43−46] By comparison, the experimental PXRD patterns of **CityU-4**, **CityU-5**, and **CityU-6** are consistent with the AB stacking mode. The experimental diffraction patterns are similar to the Pawley-refined PXRD profiles with slight differences and satisfactory convergences of R_p and R_{wp} values, clearly confirming their highly ordered structures of three COFs.
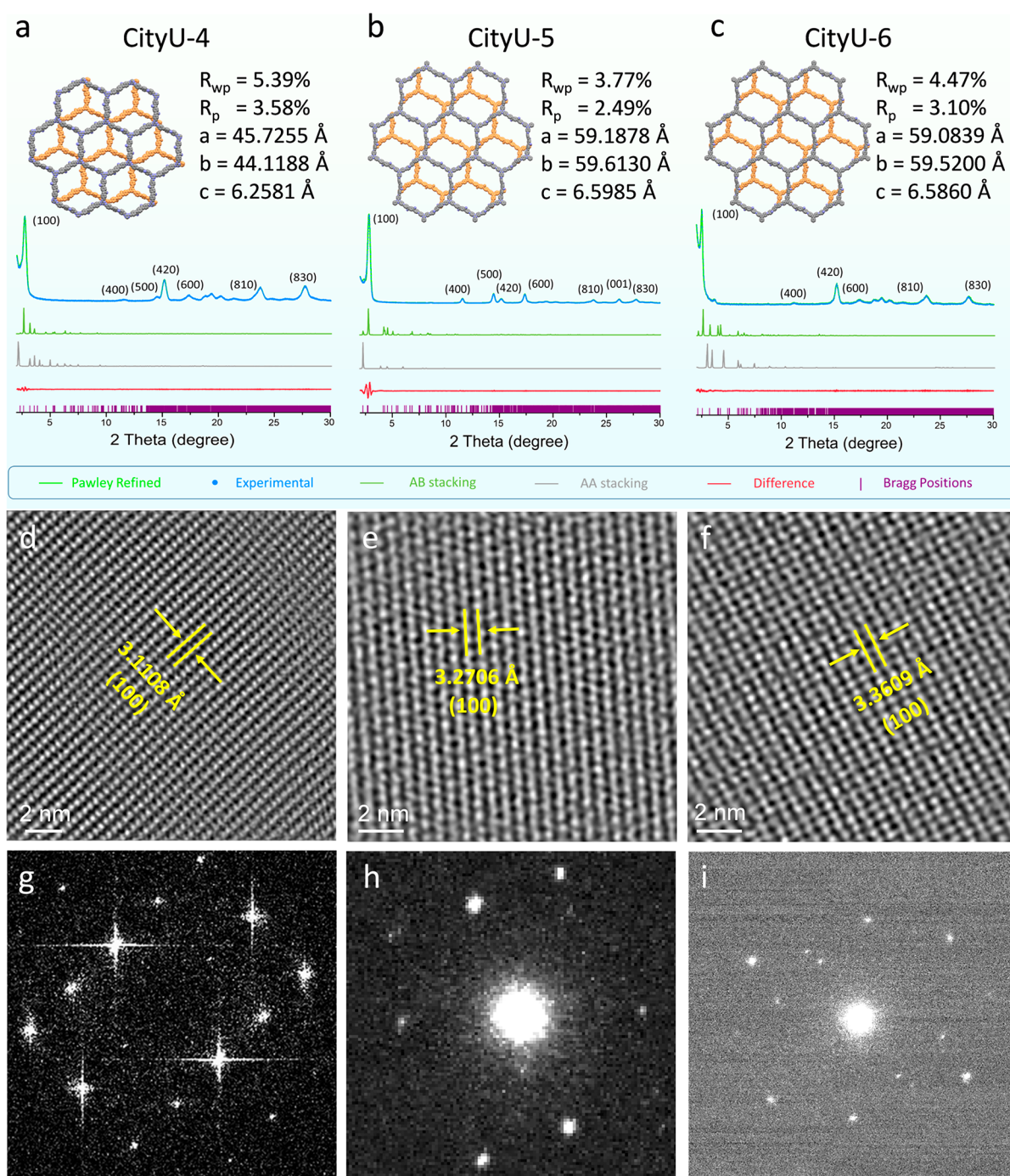
Figure 2. Lattice structures and crystallinity of three COFs. (a−c) PXRD patterns of CityU-4 (a), CityU-5 (b), and CityU-6 (c) with the corresponding AA, AB stacking modes and Pawley refined results. The insets are the reconstructed crystal structures of three COFs with the AB-stacking model along the *z* direction. (d−f) HRTEM images denoised with average background subtraction filter (ABSF) for CityU-4 (d), CityU-5 (e), and CityU-6 (f). (g−i) FFT patterns of for CityU-4 (g), CityU-5 (h), and CityU-6 (i).

The structural regularity of these three COFs was also investigated using high-resolution transmission electron microscopy (HRTEM). The periodic lattice fringes in HRTEM images (Figure S6), especially in the average background subtraction filter (ABSF)-filtered HRTEM images of **CityU-4** (Figure 2d), **CityU-5** (Figure 2e), and **CityU-6** (Figure 2f), further reveal their high structural order.[13,47−49] The lattice planes in the HRTEM images of three COFs are consistent with those from PXRD results, and the FFT patterns (Figure 2g−i) clearly show the hexagonal structural order.

Due to the as-prepared three COFs with AB stacking modes, it is reasonable to find that these COFs possess small BET surface area.[50] Moreover, the staggered stacking model of three COFs may also lead to attenuated $\pi-\pi$ stacking and result in small specific surface areas.[51−55] The permanent porosity of three COFs were studied using N_2 sorption isotherms measured at 77 K (Figure S7), displaying reversible type I isotherms for all three COFs.[56] Pore size distributions, derived from the corresponding N_2 adsorption isotherm using nonlocal density functional theory (NLDFT), indicate that the main
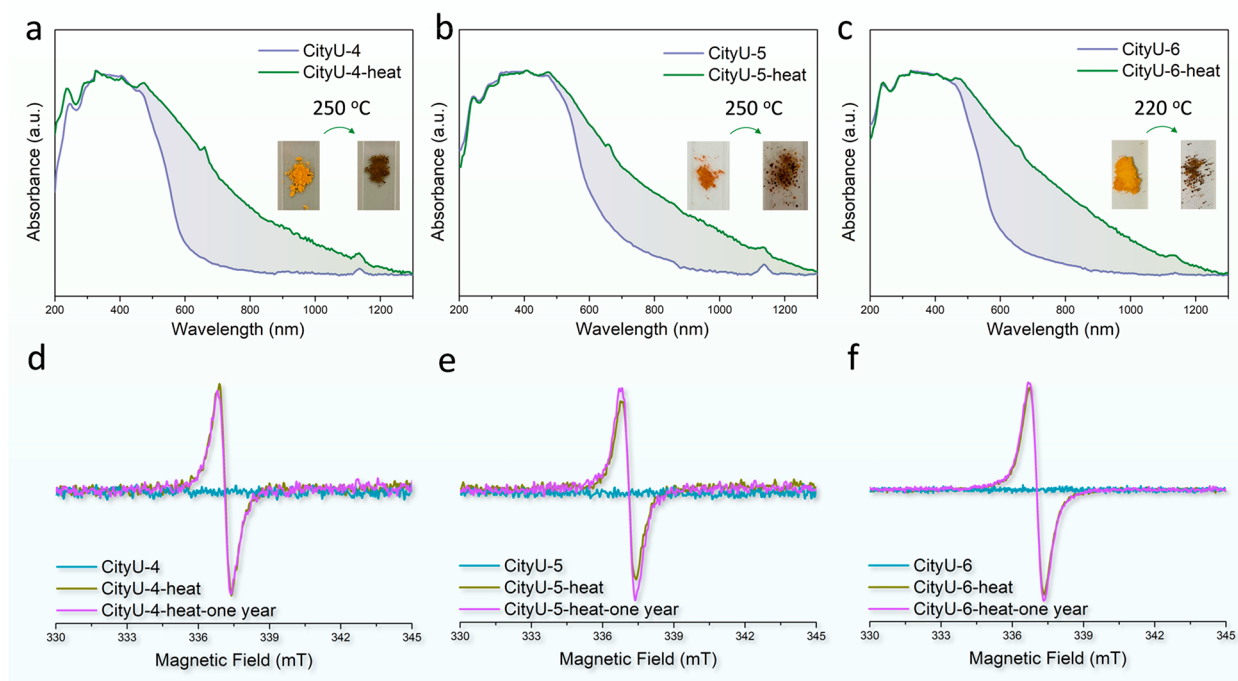
Figure 3. Thermally induced COF radicals. (a−c) UV−vis absorption spectra of CityU-4 (a), CityU-5 (b), and CityU-6 (c) with/without heat treatment. The insets are the photos of the three COFs before/after heating process in daylight. (d−f) Solid ESR signals induced by heat treatment of CityU-4 (d), CityU-5 (e), and CityU-6 (f) and their ESR intensity after one year of storage at ambient conditions.

pore sizes for **CityU-4**, **CityU-5**, and **CityU-6** are 14.8, 16.1, and 16.0 Å, respectively. The surface areas of **CityU-4**, **CityU-5**, and **CityU-6** were calculated to be 27, 47, and 64 m^2/g, respectively, using the Brunauer−Emmett−Teller (BET) approach. The specific surface areas of three COFs are much smaller than those of the simulated results without consideration of the physically adsorbates, attenuated $\pi-\pi$ stacking, and pore collapse (Figure S8). Thermogravimetric analysis (TGA) was used to evaluate their thermal stability, where **CityU-4**, **CityU-5**, and **CityU-6** exhibit good thermal stability with decomposition temperature up to 410, 406, and 325 °C, respectively (Figure S9). The absence of an endothermic or exothermic peak in differential scanning calorimetry (DSC) curves after three cycles confirmed their thermal stability in a particular temperature range (Figure S10). Since the FTIR spectra confirm the imine bonds, PXRD and HRTEM demonstrate the crystallinity and structural order, and N_2 sorption isotherms confirm the permanent porosity, we may conclude the successful synthesis of three COFs with good thermal stability.

Thermally Induced COFs Radicals. After **CityU-4** or **CityU-5** was heated at 250 °C (220 °C for **CityU-6**) for 10 min in air or 60 min in inert gas (N_2), the colors of **CityU-4** (Figure 3a inset), **CityU-5** (Figure 3b inset), and **CityU-6** (Figure 3c inset) changed from orange to dark red. The pristine COFs showed broad absorption from 200 to 600 nm. More specifically, the absorption band of **CityU-4** tailed to 608 nm (Figure 3a), while those of **CityU-5** and **CityU-6** tailed to 623 nm (Figure 3b) and 615 nm (Figure 3c), respectively. After heat treatment, visible red-shifted absorption (up to 1300 nm) was observed for all three COFs. Moreover, the quenched emission of three COFs after heat treatment also demonstrates the formation of organic radicals since the radicals could attenuate the irradiative recombination and thereby the emission would be suppressed (Figure S11). These factors

suggest the formation of radicals (Figure S12), as the unpaired electrons entail the existence of occupied α spin ("spin-up" ↑) or β spin ("spin-down" ↓) orbitals, that is, the singly occupied molecular orbital (SOMO). The SOMO spatial function and the unpaired spin are intimately connected to the radical properties with narrow band gap and long absorption wavelength.[2,4,6,57]

The thermally induced persistent COFs radicals were confirmed by ESR measurements. Pristine **CityU-4** (Figure 3d), **CityU-5** (Figure 3e) and **CityU-6** (Figure 3f) showed no ESR signals; however, after heat treatment, these samples showed strong ESR signals centered at g = 2.003, indicating the formation of radicals.[23,32,58,59] It is worth mentioning that ESR signals can still be detected without any decreased intensity even after one year under ambient conditions. The generation of COFs radicals was further elucidated by solid ^{13}C NMR spectroscopy. Peaks at 117.3 and 136.0 ppm in the ^{13}C NMR spectra, assigned to carbons adjacent to the cyano segment in three COFs (Figure S13), were superimposed on the neighboring peaks after heat treatment, indicating the occurrence of organic radicals that weaken original signals without destroying the frameworks.[60] The possibility of framework collapse during the generation of thermally induced radicals can be excluded because almost no variation was observed in the FTIR spectra after heat treatment, especially for the Schiff base (C=N) bridge connecting two building units (Figure S14). Importantly, the crystallinity of three COFs was well retained after heat treatment according to the PXRD patterns (Figure S15). Moreover, the morphology and elemental distribution did not change after heat treatment, further implying the retention of the framework structures (Figures S16−S21).

Spin polarization and Magnetization of Thermally Induced COFs Radicals. With the change in electronic structure and spin state upon heating, two very distinct
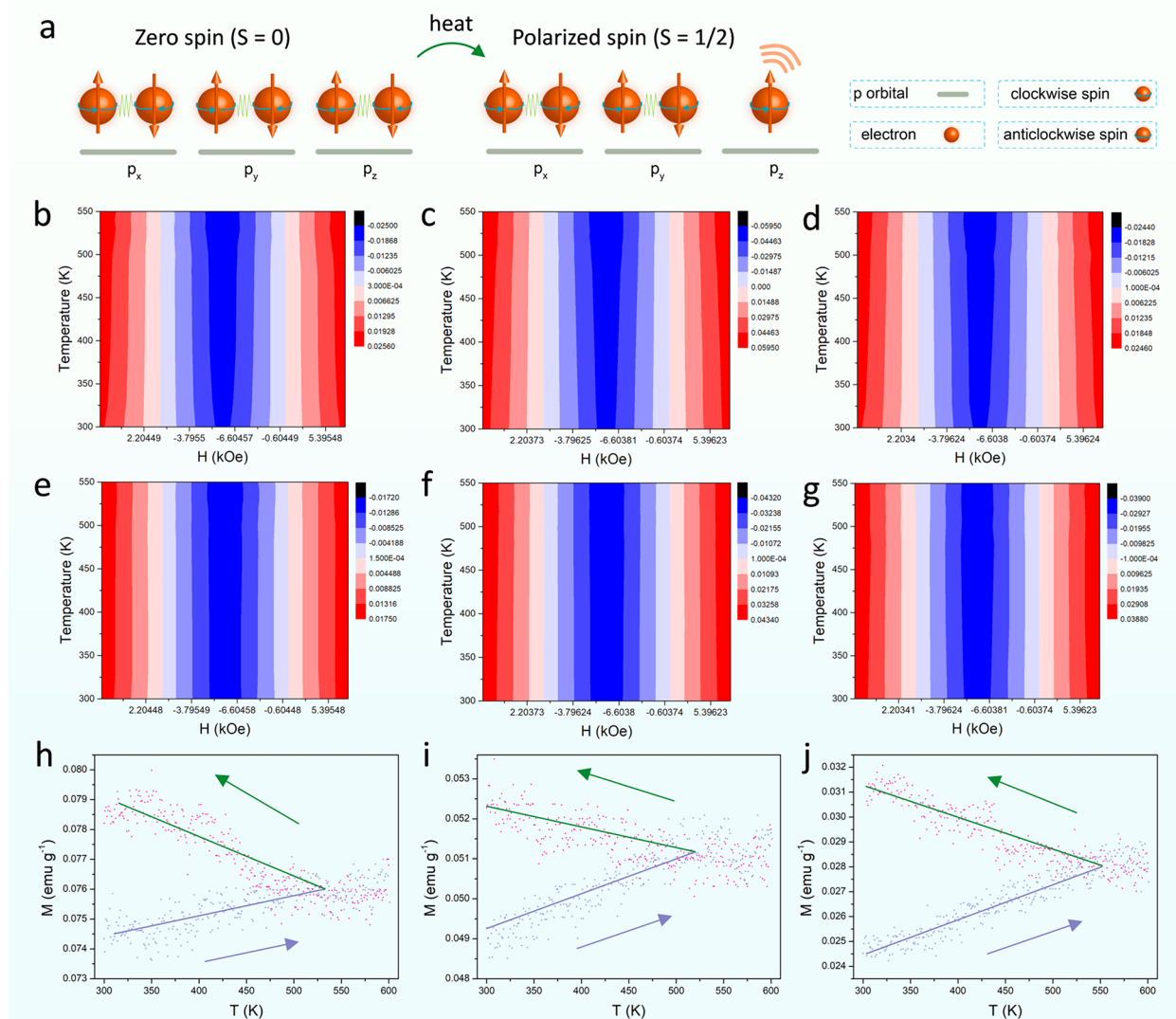
Figure 4. Spin polarization and magnetization. (a) Schematic of diamagnetic-paramagnetic transition due to $S = 1/2$ spins arising from the thermally induced unpaired p electrons in these heat-treated COFs. (b−d) Contour plots of the magnetic hysteresis (M-H) loops for CityU-4 (b), CityU-5 (c), and CityU-6 (d) measured at 10 different temperatures (300, 330, 390, 480, 500, 510, 520, 530, 540, and 550 K). (e−g) Contour plots of M-H curves for CityU-4 (e), CityU-5 (f), and CityU-6 (g) after heat treatment. (h−j) Temperature-dependent magnetization (M-T) with increasing (purple dots and line) and then decreasing (green dots and line) temperature for CityU-4 (h), CityU-5 (i), and CityU-6 (j). The purple arrows show the increase in magnetization with increasing temperature while the green arrows imply the increase in magnetization with decreasing temperature.

resonant forms, namely, the closed-shell (zero spin, $S = 0$) and open-shell radical forms (polarized spin, $S = 1/2$) were observed, leading to different spin polarizations and magnetic properties. The magnetic susceptibility measurements of all of the COFs radicals were conducted in a vibrating sample magnetometer (VSM). As illustrated in Figure 4a, the pristine COFs without unpaired electrons resulted in an antiparallel alignment of electron spins (zero spin, $S = 0$). Upon heating, a-polarized spin ($S = 1/2$) was produced due to thermally induced unpaired p electrons (radicals). These spin-polarized radicals contributed to the overall magnetic susceptibility and reduced magnetization degeneration at high temperatures. Therefore, the magnetic moments (M) of pristine CityU-4 (Figure 4b), CityU-5 (Figure 4c), and CityU-6 (Figure 4d) gradually increased when the temperature increased from 300 to 550 K due to the spin polarization of the thermally induced COFs radicals. In contrast, a negligible change in M was

observed for the heat-treated **CityU-4** (Figure 4e), **CityU-5** (Figure 4f), and **CityU-6** (Figure 4g) when increasing the temperature, due to the absence of further generated radicals. The magnetization of three thermally induced COFs radicals was further confirmed according to the temperature dependence of magnetization (M-T curves). It was clearly observed that the magnetization of **CityU-4** (Figure 4h), **CityU-5** (Figure 4i), and **CityU-6** (Figure 4j) increased stepwise with increasing temperature (purple arrows). The magnetic moments (M) continued to increase when the temperature was subsequently decreased (green arrows), leading to nonzero net magnetization. Moreover, magnetic moments were close to each other when the temperature was increased and subsequently decreased, leading to a net magnetization of zero for heat-treated COFs (Figure S22). The inconspicuous variation of M in the M-H and M-T curves for heat-treated COFs further demonstrated that the "turn-on" of the-polarized
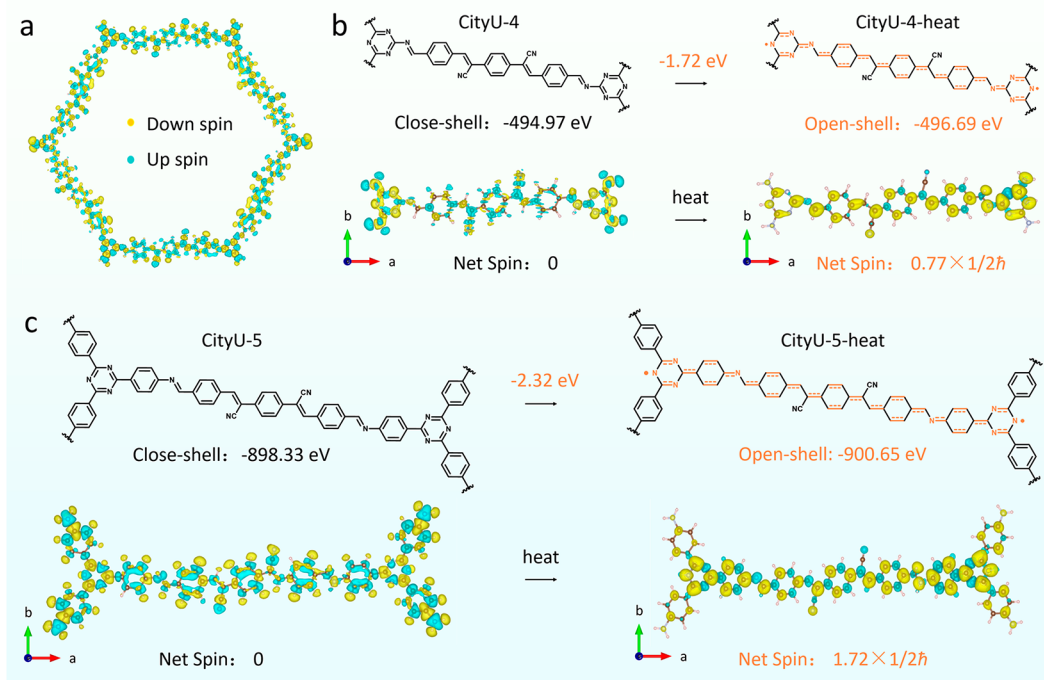
Figure 5. Theoretical calculations of spin density and total energy. (a) Spin density distribution in CityU-4. The net spin is zero. (b) Spin density distribution in one side of CityU-4 and CityU-4-heat in radical form. (c) Spin density distribution in one side of CityU-5 and CityU-5-heat with radicals. CityU-4-heat and CityU-5-heat in radical forms possess the lower energy state with a net spin of $0.77 \times 1/2\hbar$ and $1.72 \times 1/2\hbar$, respectively. The isosurface value for the spin density distribution is set as 0.004 e Å^{-3}.

spin during heating was ascribed to the generation of persistent COF radicals.

Mechanism of persistent COFs Radicals by Theoretical Calculations. To gain deeper insight into the thermally induced radicals and associated magnetization, spin-polarized density functional theory (DFT) calculations of the total energy and net spin density were employed, where **CityU-4** and **CityU-5** were chosen as examples. The pristine **CityU-4** with a closed-shell form exhibited no net spin (Figure 5a). By analysis of one side of the hexagon scaffold in **CityU-4**, the spin polarization was also zero (Figure 5b). However, after heat treatment, a net spin of $0.77 \times 1/2\hbar$ was generated for **CityU-4-heat** with an open-shell radical form (Figure 5b), where the singlet/triplet ratio of COFs radical is 0.237/0.763 due to radicals with spin polarization.[39] Moreover, the total energies of **CityU-4** and **CityU-4-heat** are −494.97 and −496.69 eV, respectively, illustrating that the transition from **CityU-4** with a higher energy to **CityU-4-heat** with a lower energy was favorable when increasing the temperature. The energy difference between **CityU-4** and **CityU-4-heat** was much larger than thermal energy; thus, **CityU-4-heat** could not spontaneously transfer back to **CityU-4** when decreasing the temperature. **CityU-5-heat** was also in a lower energy state with a net spin of $1.72 \times 1/2\hbar$ (Figure 5c). The singlet/triplet radical ratio is 0.120/0.880, where triplet species are also dominant. Even if the energy of the open-shell form is lower than that of the closed-shell conformer, there would be a transition state between a higher-energy closed-shell form and a lower-energy open-shell conformer. To overcome the high energy barrier between the initial state and the transition state, heat treatment is necessary to provide sufficient energy and benefit the transition from the closed-shell from to the open-shell conformer.[61] The transition state after heat treatment

entails the optimized planarity, benefiting the formation of organic radicals.[62,63]

CONCLUSION

In summary, three *p*-phenylenediacetonitrile-based isoreticular COFs (**CityU-4**, **CityU-5**, and **CityU-6**) were successfully constructed. Heating these COFs at relatively high temperatures evokes the delocalization of unpaired electrons and transition from the closed-shell form to the open-shell radical form. The thermally induced COFs radicals were identified by visible color changes, red-shifted absorption, and solid ^{13}C NMR spectra. Furthermore, ESR spectra with an intense signal centralized at $g = 2.003$ for heat-treated COFs confirm the formation of the COFs radicals. These COF radicals are persistent and could be detected even after one year without any decrease in ESR intensity. According to DFT simulation, the lower energy and nonzero spin density contributes to the stability and spin polarization of the thermally induced COFs radicals. Interestingly, the spin polarization of thermally induced COFs radicals contributes to the magnetic susceptibility. Our work provides an alternative and facile approach to generate persistent COF radicals for further photoelectronic and magnetic applications.

METHODS/EXPERIMENTAL DETAILS

Synthesis of 3B2CN. Terephthalaldehyde (7.6 mmol, 1.020 g) and 1,4-phenylenediacetonitrile (3.8 mmol, 594 mg) were loaded into a 100 mL round-bottomed flask (RBF) before adding 40 mL of ethanol (EtOH), several drops of DI water, and piperidine. The mixture was refluxed for 24 h and then cooled to room temperature. The precipitate was filtered and washed by EtOH several times to afford the target product.

Synthesis of CityU-4. 6.3 mg of melamine (MA, 0.05 mmol) was ultrasonically dissolved in 0.5 mL of superdry 1,4-dioxane to form

solution A. In the pyrex tube, 30 mg of 3B2CN (0.075 mmol) was dispersed in 0.5 mL of superdry 1,4-dioxane with the addition of 120 μL of aniline and 200 μL of aqueous acetic acid solution (6 mol/L) to form solution B. Then, solution A was injected into solution B before sonicating for a while. The mixture was degassed through three freeze—pump—thaw cycles before being sealed under vacuum. The sealed tube was put into the oven at 150 °C for 72 h before cooling to room temperature. The obtained precipitate was filtered and washed with *N,N*-dimethylformamide (DMF), dichloromethane (DCM), acetone and *n*-hexane subsequently. Each sample was washed several times before Soxhlet extraction in tetrahydrofuran (THF) overnight. Then, the precipitate was dried under vacuum to afford **CityU-4**.

Synthesis of CityU-5. The synthesis of **CityU-5** was similar to that of CityU-4; however, solution A was prepared by adding 18 mg of tris(4-aminophenyl)triazine (TAPT, 0.05 mmol) in 0.5 mL of superdry 1,4-dioxane. The washing process was the same to that of **CityU-4**.

Synthesis of CityU-6. The synthesis of **CityU-6** was similar to that of **CityU-4**, except that solution A was formed by loading 18 mg of 1,3,5-tris(4-aminophenyl)benzene (TAPB, 0.05 mmol) in 0.5 mL of superdry 1,4-dioxane. The washing process was the same to that of **CityU-4**.

Heating Treatment. The temperature ranges in the DSC curves are the indicators for the heating treatment of three COFs. **CityU-4-heat** samples were obtained by heating **CityU-4** at 250 °C for 60 min in N_2 atmosphere. Prior to that, **CityU-4** was loaded into a pyrex tube and degassed through vacuum-N_2 purge cycles for sealing. **CityU-4-heat** samples can also be obtained after loading **CityU-4** onto glass slide and heating at 250 °C for 10 min in air. **CityU-5-heat** samples were obtained with the same process while **CityU-6-heat** samples were obtained with lower temperature (220 °C) according to the DSC curves.

Characterization. Fourier transform infrared (FTIR) spectra from 400 to 4000 cm^{-1} were collected from a PerkinElmer Spectrum Two spectrometer with an attenuated total reflection (ATR) mode. ^1H NMR spectra were obtained from a Bruker 400 MHz "AVANCE III" Nuclear Magnetic Resonance spectrometer, where tetramethylsilane (TMS) was used as the internal standard. ^{13}C cross-polarization/magic-angle spinning (CP/MAS) solid-state nuclear magnetic resonance (NMR) spectra were measured by using a Bruker 600 MHz "ASCED AVANCE III HD" Nuclear Magnetic Resonance spectrometer. Transmission electron microscopy (TEM) and high-resolution transmission electron microscopy (HRTEM) images were captured on a transmission electron microscope (JEOL JEM-2100F) at an accelerating voltage of 200 kV. Prior to the TEM characterizations, three COFs were dispersed in ethanol by sonication to form the suspension before dropping onto the carbon support copper grids, and then dried in air naturally. Scanning electron microscopy (SEM) images and elemental mappings of three COFs were recorded on a Quattro S scanning electron microscope of Thermo Fisher. Powder X-ray diffraction (PXRD) patterns were recorded at 30 kV and 10 mA with a scan rate of 0.1°/s on a Rigaku X-ray Diffractometer (SmartLabTM 9 kW) with Cu Kα monochromatic radiation source (λ = 1.5406 Å). Thermogravimetric analysis (TGA) was performed on a PerkinElmer Simultaneous Thermal Analyzer (STA) 6000 with a heating rate of 10 °C/min under N_2 atmosphere. Differential Scanning Calorimetry (DSC) was measured on a PerkinElmer Differential Scanning Calorimeter 8000 with a heating rate of 10 °C/min. All three COFs were degassed at 120 °C for 12 h before testing the nitrogen sorption isotherms on a Micromeritics 3Flex 3500 Multiport High Throughput Gas Adsorption Analyzer at 77 K. The surface areas were evaluated by applying the Brunauer—Emmett—Teller (BET) approach. Simultaneously, the pore size distributions for the three COFs were derived from the corresponding N_2 adsorption isotherm by using the nonlocal density functional theory (NLDFT) method. UV—vis absorption spectra were captured using a Hitachi UH4150 UV—vis—NIR spectrophotometer by setting wavelength from 200 to 1300 nm. Fluorescence spectra were collected on a Horiba FluoroMax-4 fluorescence spectrometer with wavelength ranging from 480 to 760 nm. Solid electron spin resonance (ESR)

spectra were collected on a Continuous wave X-band JEOL JES-FA200 spectrometer at room temperature (293 K). The magnetic characterization was performed using a vibrating sample magnetometer (VSM, LakeShore 8600), and the background signals were detected before starting to measure the samples in order to exclude the interference from ferromagnetic components and other factors. The measurement parameters of the M-H curve were as follows. The max field was 8 kOe, field step size was 200 Oe, averaging time was 5 s, and the pause after initial ramp was 1 s. The M-T curve was measured via variable temperature accessories (SSVT, 270 K-700 K), and the measurement parameters were as follow. The begin temperature was 300 K, end temperature was 600 K, and the temperature step size was 1 degree.

Structure Determination. Molecular modeling of three COFs was performed by using Materials Studio (MS) 2020 suite of programs (BIOVIA). P1 unit cells conceived from the native connectivity and geometry of the building blocks were used for modeling three COFs. The initial COF structure was geometrically optimized using Forcite molecular dynamics module (Universal force fields, Ewald summations) in MS.[43] Typical AA- and AB-stacking models were constructed for structural simulation. Pawley refinements were also carried out using implemented Reflex package in MS 2020 with the XRD patterns and optimized COF structures. The lattice parameters were iteratively optimized with $a = b$, $\alpha = \beta = 90°$, and $\gamma = 120°$ until the R_p and R_{wp} values converged.

Computational Details. Spin-polarized density functional theory (DFT) calculations were carried out using a Vienna ab initio simulation package (VASP). The projected augmented wave (PAW) method was used to describe electron—ion interactions. The exchange—correlation interaction was treated by the generalized gradient approximation (GGA) in the form of the Perdew—Burke—Ernzerhof (PBE) functional. The cutoff energy of the plane wave was 450 eV. A k-grid of $3 \times 3 \times 4$ was employed in the electronic structure calculations. The convergence criteria for energy and force were set to 1×10^{-5} eV and 0.01 eV/Å, respectively.

ASSOCIATED CONTENT

Ⓢ Supporting Information

The Supporting Information is available free of charge at https://pubs.acs.org/doi/10.1021/acsnano.3c08313.

Synthesis of COF precursor 3B2CN, synthesis and characterization of three pristine COFs (**CityU-4**, **CityU-5**, and **CityU-6**), heating treatment of three COFs, structure determination of three COFs by using Materials Studio (MS); spin-polarized density functional theory (DFT) calculations using a Vienna ab initio simulation package (VASP); FTIR spectra and XRD patterns of three COFs with their precursors as comparison; TEM images, N_2 sorption isotherms, simulated porosity and specific surface area, TGA curves and DSC curves of three COFs; emission spectra, solid ^{13}C NMR spectra, FTIR spectra, PXRD patterns, and SEM images of three COFs with/without heating treatment, ^1H NMR spectra, atomic coordinates (PDF)

AUTHOR INFORMATION

Corresponding Authors

Wei Qin — *School of Physics, State Key Laboratory of Crystal Materials, Shandong University, Jinan 250100, P. R. China;* ⓞ orcid.org/0000-0003-4579-0061; Email: wqin@sdu.edu.cn

Yu Han — *Advanced Membranes and Porous Materials (AMPM) Center, Physical Science and Engineering Division, King Ab-dullah University of Science and Technology*

(KAUST), Thuwal 23955-6900, Saudi Arabia; orcid.org/0000-0003-1462-1118; Email: yu.han@kaust.edu.sa

Xiaogang Liu − Department of Chemistry and the N.1 Institute for Health, National University of Singapore, Singapore 117543, Singapore; orcid.org/0000-0003-2517-5790; Email: chmlx@nus.edu.sg

Qichun Zhang − Department of Materials Science and Engineering, City University of Hong Kong, Kowloon, Hong Kong SAR 999077, P. R. China; Department of Chemistry & Center of Super-Diamond and Advanced Films (COSDAF) and Department of Chemistry, City University of Hong Kong, Kowloon, Hong Kong SAR 999077, P. R. China; orcid.org/0000-0003-1854-8659; Email: qiczhang@cityu.edu.hk

Authors

Qianfeng Gu − Department of Materials Science and Engineering, City University of Hong Kong, Kowloon, Hong Kong SAR 999077, P. R. China

Xiangqian Lu − School of Physics, State Key Laboratory of Crystal Materials, Shandong University, Jinan 250100, P. R. China

Cailing Chen − Advanced Membranes and Porous Materials (AMPM) Center, Physical Science and Engineering Division, King Ab-dullah University of Science and Technology (KAUST), Thuwal 23955-6900, Saudi Arabia; orcid.org/0000-0003-2598-1354

Renjie Hu − School of Physics, State Key Laboratory of Crystal Materials, Shandong University, Jinan 250100, P. R. China

Xin Wang − Department of Materials Science and Engineering, City University of Hong Kong, Kowloon, Hong Kong SAR 999077, P. R. China

Guohan Sun − Department of Chemistry, City University of Hong Kong, Kowloon, Hong Kong SAR 999077, P. R. China

Fangyuan KANG − Department of Materials Science and Engineering, City University of Hong Kong, Kowloon, Hong Kong SAR 999077, P. R. China

Jinglun Yang − Department of Materials Science and Engineering, City University of Hong Kong, Kowloon, Hong Kong SAR 999077, P. R. China

Xiang Wang − Department of Materials Science and Engineering, City University of Hong Kong, Kowloon, Hong Kong SAR 999077, P. R. China

Jinghang Wu − Department of Materials Science and Engineering, City University of Hong Kong, Kowloon, Hong Kong SAR 999077, P. R. China

Yang Yang Li − Department of Materials Science and Engineering, City University of Hong Kong, Kowloon, Hong Kong SAR 999077, P. R. China; orcid.org/0000-0003-4153-9558

Yung-Kang Peng − Department of Chemistry, City University of Hong Kong, Kowloon, Hong Kong SAR 999077, P. R. China; orcid.org/0000-0001-9590-6902

Complete contact information is available at:
https://pubs.acs.org/10.1021/acsnano.3c08313

Author Contributions

Q.Z., Xiaogang Liu, Y.H., and W.Q. designed and conceived the project. Q.G. synthesized the compounds and collected the spectral data. Xiangqian Lu did magnetic measurements and analysis. C.C. collected the TEM images. R.H. conducted the theoretical calculations on spin density. Xin Wang performed simulation of stacking structures and Pawley refinement on those structures. Q.G., G.S., and Y-K.P. collected the ESR spectra. Q.G., F.K., J.Y., Xiang Wang, and J.W. did the X-ray analysis. Q.G. and Y.Y.L. did the absorption spectral measurement and analysis. Q.G., Q.Z., Xiaogang Liu, Y.H., and W.Q. participated in the discussion of results and manuscript writing. Q.G., Xiangqian Lu, and C.C. contributed equally to this work.

Notes

The authors declare no competing financial interest.

REFERENCES

(1) Song, S.; Guo, N.; Li, X.; Li, G.; Haketa, Y.; Telychko, M.; Su, J.; Lyu, P.; Qiu, Z.; Fang, H.; et al. Real-Space Imaging of a Single-Molecule Monoradical Reaction. J. Am. Chem. Soc. 2020, 142, 13550−13557.

(2) Kasemthaveechok, S.; Abella, L.; Crassous, J.; Autschbach, J.; Favereau, L. Organic radicals with inversion of SOMO and HOMO energies and potential applications in optoelectronics. Chem. Sci. 2022, 13, 9833−9847.

(3) Zhang, H.; Phan, H.; Herng, T. S.; Gopalakrishna, T. Y.; Zeng, W.; Ding, J.; Wu, J. Conformationally Flexible Bis(9-fluorenylidene)-porphyrin Diradicaloids. Angew. Chem., Int. Ed. 2017, 56, 13484−13488.

(4) Su, Y.; Chen, Z.; Tang, X.; Xu, H.; Zhang, Y.; Gu, C. Design of Persistent and Stable Porous Radical Polymers by Electronic Isolation Strategy. Angew. Chem., Int. Ed. 2021, 60, 24424−24429.

(5) Chen, Z. X.; Li, Y.; Huang, F. Persistent and Stable Organic Radicals: Design, Synthesis, and Applications. Chem. 2021, 7, 288−332.

(6) Li, Y.; Li, L.; Wu, Y.; Li, Y. A Review on the Origin of Synthetic Metal Radical: Singlet Open-Shell Radical Ground State? J. Phys. Chem. C 2017, 121, 8579−8588.

(7) Ye, X.; Chung, L.-H.; Li, K.; Zheng, S.; Wong, Y.-L.; Feng, Z.; He, Y.; Chu, D.; Xu, Z.; Yu, L.; He, J.; et al. Organic radicals stabilization above 300 oC in Eu-based coordination polymers for solar steam generation. Nat. Commun. 2022, 13, 6116.

(8) Kang, F.; Wang, X.; Chen, C.; Lee, C. S.; Han, Y.; Zhang, Q. Construction of Crystalline Nitrone-Linked Covalent Organic Frame-works Via Krohnke Oxidation. J. Am. Chem. Soc. 2023, 145, 15465−15472.

(9) Doonan, C. J.; Tranchemontagne, D. J.; Glover, T. G.; Hunt, J. R.; Yaghi, O. M. Exceptional ammonia uptake by a covalent organic framework. Nat. Chem. 2010, 2, 235−238.

(10) Zhang, H.; Lin, Z.; Kidkhunthod, P.; Guo, J. Stable Immobilization of Nickel Ions on Covalent Organic Frameworks for Panchromatic Photocatalytic Hydrogen Evolution. Angew. Chem., Int. Ed. 2023, 62, No. e202217527.

(11) Liu, X.; Qi, R.; Li, S.; Liu, W.; Yu, Y.; Wang, J.; Wu, S.; Ding, K.; Yu, Y. Triazine-Porphyrin-Based Hyperconjugated Covalent Organic Framework for High-Performance Photocatalysis. J. Am. Chem. Soc. 2022, 144, 23396−23404.

(12) You, Z.; Wang, B.; Zhao, Z.; Zhang, Q.; Song, W.; Zhang, C.; Long, X.; Xia, Y. Metal-Free Carbon-Based Covalent Organic

Frameworks with Heteroatom-Free Units Boost Efficient Oxygen Reduction. *Adv. Mater.* **2023**, *35*, No. e2209129.

(13) Duan, H.; Li, K.; Xie, M.; Chen, J. M.; Zhou, H. G.; Wu, X.; Ning, G. H.; Cooper, A. I.; Li, D. Scalable Synthesis of Ultrathin Polyimide Covalent Organic Framework Nanosheets for High-Performance Lithium-Sulfur Batteries. *J. Am. Chem. Soc.* **2021**, *143*, 19446−19453.

(14) Yang, Y.; Sandra, A. P.; Idstrom, A.; Schafer, C.; Andersson, M.; Evenas, L.; Borjesson, K. Electroactive Covalent Organic Framework Enabling Photostimulus-Responsive Devices. *J. Am. Chem. Soc.* **2022**, *144*, 16093−16100.

(15) Gu, Q.; Zha, J.; Chen, C.; Wang, X.; Yao, W.; Liu, J.; Kang, F.; Yang, J.; Li, Y. Y.; Lei, D.; Tang, Z.; Han, Y.; Tan, C.; Zhang, Q. Constructing Chiral Covalent-Organic Frameworks for Circularly-polarized Light Detection. *Adv. Mater.* **2023**, DOI: 10.1002/adma.202306414.

(16) Sun, J.; Xu, Y.; Lv, Y.; Zhang, Q.; Zhou, X. Recent Advances in Covalent Organic Framework Electrode Materials for Alkali Metal-Ion Batteries. *CCS Chem.* **2023**, *5*, 1259−1276.

(17) Shi, Y.; Yang, J.; Gao, F.; Zhang, Q. Covalent Organic Frameworks: Recent Progress in Biomedical Applications. *ACS Nano* **2023**, *17*, 1879−1905.

(18) She, P.; Qin, Y.; Wang, X.; Zhang, Q. Recent Progress in External-Stimulus-Responsive 2D Covalent Organic Frameworks. *Adv. Mater.* **2022**, *34*, No. e2101175.

(19) Liu, Y. Y.; et al. Self-templated synthesis of uniform hollow spheres based on highly conjugated three-dimensional covalent organic frameworks. *Nat. Commun.* **2020**, *11*, 5561.

(20) Liu, X.; Liu, C.-F.; Xu, S.; Cheng, T.; Wang, S.; Lai, W.-Y.; Huang, W. Porous organic polymers for high-performance super-capacitors. *Chem. Soc. Rev.* **2022**, *51*, 3181−3225.

(21) Wang, S.; Li, X.; Cheng, T.; Liu, Y.; Li, Q.; Bai, M.; Liu, X.; Geng, H.; Lai, W.-Y.; Huang, W. Highly conjugated three-dimensional covalent organic frameworks with enhanced Li-ion conductivity as solid-state electrolytes for high-performance lithium metal batteries. *J. Mater. Chem. A* **2022**, *10*, 8761−8771.

(22) Wang, M.; Wang, G.; Naisa, C.; Fu, Y.; Gali, S. M.; Paasch, S.; Wang, M.; Wittkaemper, H.; Papp, C.; Brunner, E.; Zhou, S.; Beljonne, D.; Steinrück, H.-P.; Dong, R.; Feng, X. Poly-(benzimidazobenzophenanthroline)-Ladder-Type Two-Dimensional Conjugated Covalent Organic Framework for Fast Proton Storage. *Angew. Chem., Int. Ed.* **2023**, *62*, e202310937.

(23) Phan, H.; Herng, T. S.; Wang, D.; Li, X.; Zeng, W.; Ding, J.; Loh, K. P.; Shen Wee, A. T.; Wu, J. Room-Temperature Magnets Based on 1,3,5-Triazine-Linked Porous Organic Radical Frameworks. *Chem.* **2019**, *5*, 1223−1234.

(24) Mahmood, J.; Park, J.; Shin, D.; Choi, H.-J.; Seo, J.-M.; Yoo, J.-W.; Baek, J.-B. Organic Ferromagnetism: Trapping Spins in the Glassy State of an Organic Network Structure. *Chem.* **2018**, *4*, 2357−2369.

(25) Liu, M.; Liu, J.; Li, J.; Zhao, Z.; Zhou, K.; Li, Y.; He, P.; Wu, J.; Bao, Z.; Yang, Q.; Yang, Y.; Ren, Q.; Zhang, Z. Blending Aryl Ketone in Covalent Organic Frameworks to Promote Photoinduced Electron Transfer. *J. Am. Chem. Soc.* **2023**, *145*, 9198−9206.

(26) Liu, X.; Li, H.; Zhang, W.; Yang, Z.; Li, D.; Liu, M.; Jin, K.; Wang, L.; Yu, G. Magnetoresistance in Organic Spin Valves Based on Acid-Exfoliated 2D Covalent Organic Frameworks Thin Films. *Angew. Chem., Int. Ed.* **2023**, *62*, e202308921.

(27) Li, Z.; Zhang, Z.; Nie, R.; Li, C.; Sun, Q.; Shi, W.; Chu, W.; Long, Y.; Li, H.; Liu, X. Construction of Stable Donor-Acceptor Type Covalent Organic Frameworks as Functional Platform for Effective Perovskite Solar Cell Enhancement. *Adv. Funct. Mater.* **2022**, *32*, 2112553.

(28) Yuan, D.; Guo, Y.; Zeng, Y.; Fan, Q.; Wang, J.; Yi, Y.; Zhu, X. Air-stable n-type thermoelectric materials enabled by organic diradicaloids. *Angew. Chem., Int. Ed.* **2019**, *58*, 4958−4962.

(29) Chen, F.; Guan, X.; Li, H.; Ding, J.; Zhu, L.; Tang, B.; Valtchev, V.; Yan, Y.; Qiu, S.; Fang, Q. Three-Dimensional Radical Covalent Organic Frameworks as Highly Efficient and Stable Catalysts for

Selective Oxidation of Alcohols. *Angew. Chem., Int. Ed.* **2021**, *60*, 22230−22235.

(30) Xu, F.; Xu, H.; Chen, X.; Wu, D.; Wu, Y.; Liu, H.; Gu, C.; Fu, R.; Jiang, D. Radical covalent organic frameworks: a general strategy to immobilize open-accessible polyradicals for high-performance capacitive energy storage. *Angew. Chem., Int. Ed.* **2015**, *54*, 6814−6818.

(31) Lakshmi, V.; Liu, C. H.; Rajeswara Rao, M.; Chen, Y.; Fang, Y.; Dadvand, A.; Hamzehpoor, E.; Sakai-Otsuka, Y.; Stein, R. S.; Perepichka, D. F. A Two-Dimensional Poly(azatriangulene) Covalent Organic Framework with Semiconducting and Paramagnetic States. *J. Am. Chem. Soc.* **2020**, *142*, 2155−2160.

(32) Mi, Z.; Yang, P.; Wang, R.; Unruangsri, J.; Yang, W.; Wang, C.; Guo, J. Stable Radical Cation-Containing Covalent Organic Frameworks Exhibiting Remarkable Structure-Enhanced Photothermal Conversion. *J. Am. Chem. Soc.* **2019**, *141*, 14433−14442.

(33) Chen, Z.; Wang, J.; Hao, M.; Xie, Y.; Liu, X.; Yang, H.; Waterhouse, G. I. N.; Wang, X.; Ma, S. Tuning excited state electronic structure and charge transport in covalent organic frameworks for enhanced photocatalytic performance. *Nat. Commun.* **2023**, *14*, 1106.

(34) Jiang, Y.; Oh, I.; Joo, S. H.; Buyukcakir, O.; Chen, X.; Lee, S. H.; Huang, M.; Seong, W. K.; Kim, J. H.; Rohde, J. U.; et al. Organic Radical-Linked Covalent Triazine Framework with Paramagnetic Behavior. *ACS Nano* **2019**, *13*, 5251−5258.

(35) Wu, S.; Li, M.; Phan, H.; Wang, D.; Herng, T. S.; Ding, J.; Lu, Z.; Wu, J. Toward Two-Dimensional π-Conjugated Covalent Organic Radical Frameworks. *Angew. Chem., Int. Ed.* **2018**, *57*, 8007−8011.

(36) Su, Y.; Wang, X.; Wang, L.; Zhang, Z.; Wang, X.; Song, Y.; Power, P. P. Thermally controlling the singlet-triplet energy gap of a diradical in the solid state. *Chem. Sci.* **2016**, *7*, 6514−6518.

(37) Wentrup, C.; Regimbald-Krnel, M. J.; Muller, D.; Comba, P. A Thermally Populated, Perpendicularly Twisted Alkene Triplet Diradical. *Angew. Chem., Int. Ed.* **2016**, *55*, 14600−14605.

(38) Rudebusch, G. E.; Zafra, J. L.; Jorner, K.; Fukuda, K.; Marshall, J. L.; Arrechea-Marcos, I.; Espejo, G. L.; Ponce Ortiz, R.; Gómez-García, C. J.; Zakharov, L. N.; et al. Diindeno-fusion of an anthracene as a design strategy for stable organic biradicals. *Nat. Chem.* **2016**, *8*, 753−759.

(39) Ma, L.; Wang, S.; Li, Y.; Shi, Q.; Xie, W.; Chen, H.; Wang, X.; Zhu, W.; Jiang, L.; Chen, R.; Peng, Q.; Huang, H. Air Stable Chalcogen-Doped Rubicenes with Diradical Character. *CCS Chem.* **2022**, *4*, 3669−3676.

(40) Guo, J.; Li, Z.; Zhang, J.; Li, B.; Liang, Y.; Wang, Y.; Xie, S.; Phan, H.; Herng, T. S.; Ding, J.; Wu, J.; Tang, B. Z.; Zeng, Z. Stable Quadruple Helical Tetraradicaloid with Thermally Induced Intra-molecular Magnetic Switching. *CCS Chem.* **2022**, *4*, 95−103.

(41) Lekin, K.; Phan, H.; Winter, S. M.; Wong, J. W.; Leitch, A. A.; Laniel, D.; Yong, W.; Secco, R. A.; Tse, J. S.; Desgreniers, S.; Dube, P. A.; Shatruk, M.; Oakley, R. T. Heat, pressure and light-induced interconversion of bisdithiazolyl radicals and dimers. *J. Am. Chem. Soc.* **2014**, *136*, 8050−8062.

(42) Chen, H.; Gu, Z. G.; Zhang, J. Chiral-Induced Ultrathin Covalent Organic Frameworks Nanosheets with Tunable Circularly-polarized Luminescence. *J. Am. Chem. Soc.* **2022**, *144*, 7245−7252.

(43) *Materials studio*; BIOVIA, **2010**.

(44) Li, L.; Yun, Q.; Zhu, C.; Sheng, G.; Guo, J.; Chen, B.; Zhao, M.; Zhang, Z.; Lai, Z.; Zhang, X.; Peng, Y.; Zhu, Y.; Zhang, H. Isoreticular Series of Two-Dimensional Covalent Organic Frameworks with the kgd Topology and Controllable Micropores. *J. Am. Chem. Soc.* **2022**, *144*, 6475−6482.

(45) Peng, Y.; Huang, Y.; Zhu, Y.; Chen, B.; Wang, L.; Lai, Z.; Zhang, Z.; Zhao, M.; Tan, C.; Yang, N.; Shao, F.; Han, Y.; Zhang, H. Ultrathin Two-Dimensional Covalent Organic Framework Nano-sheets: Preparation and Application in Highly Sensitive and Selective DNA Detection. *J. Am. Chem. Soc.* **2017**, *139*, 8698−8704.

(46) Jin, E.; Geng, K.; Fu, S.; Addicoat, M. A.; Zheng, W.; Xie, S.; Hu, J. S.; Hou, X.; Wu, X.; Jiang, Q.; Xu, Q.-H.; Wang, H. I.; Jiang, D. Module-Patterned Polymerization towards Crystalline 2D sp^2

-Carbon Covalent Organic Framework Semiconductors. *Angew. Chem., Int. Ed.* **2022**, *61*, No. e202115020.

(47) Liu, W.; Li, X.; Wang, C.; Pan, H.; Liu, W.; Wang, K.; Zeng, Q.; Wang, R.; Jiang, J. A Scalable General Synthetic Approach toward Ultrathin Imine-Linked Two-Dimensional Covalent Organic Framework Nanosheets for Photocatalytic CO_2 Reduction. *J. Am. Chem. Soc.* **2019**, *141*, 17431−17440.

(48) Han, B.; Jin, Y.; Chen, B.; Zhou, W.; Yu, B.; Wei, C.; Wang, H.; Wang, K.; Chen, Y.; Chen, B.; Jiang, J. Maximizing Electroactive Sites in a Three-Dimensional Covalent Organic Framework for Significantly Improved Carbon Dioxide Reduction Electrocatalysis. *Angew. Chem., Int. Ed.* **2022**, *61*, No. e202114244.

(49) Bi, S.; Yang, C.; Zhang, W.; Xu, J.; Liu, L.; Wu, D.; Wang, X.; Han, Y.; Liang, Q.; Zhang, F. Two-dimensional semiconducting covalent organic frameworks via condensation at arylmethyl carbon atoms. *Nat. Commun.* **2019**, *10*, 2467.

(50) Yang, Z.; Chen, H.; Wang, S.; Guo, W.; Wang, T.; Suo, X.; Jiang, D. E.; Zhu, X.; Popovs, I.; Dai, S. Transformation Strategy for Highly Crystalline Covalent Triazine Frameworks: From Staggered AB to Eclipsed AA Stacking. *J. Am. Chem. Soc.* **2020**, *142*, 6856−6860.

(51) Jin, F.; Wang, T.; Zheng, H.; Lin, E.; Zheng, Y.; Hao, L.; Wang, T.; Chen, Y.; Cheng, P.; Yu, K.; Zhang, Z. Bottom-Up Synthesis of Covalent Organic Frameworks with Quasi-Three-Dimensional Integrated Architecture via Interlayer Cross-Linking. *J. Am. Chem. Soc.* **2023**, *145*, 6507−6515.

(52) Feriante, C. H.; Jhulki, S.; Evans, A. M.; Dasari, R. R.; Slicker, K.; Dichtel, W. R.; Marder, S. R. Rapid Synthesis of High Surface Area Imine-Linked 2D Covalent Organic Frameworks by Avoiding Pore Collapse During Isolation. *Adv. Mater.* **2020**, *32*, No. e1905776.

(53) Xu, H.; Gao, J.; Jiang, D. Stable, crystalline, porous, covalent organic frameworks as a platform for chiral organocatalysts. *Nat. Chem.* **2015**, *7*, 905−912.

(54) Dodson, R. A.; Wong-Foy, A. G.; Matzger, A. J. The Metal-Organic Framework Collapse Continuum: Insights from Two-Dimensional Powder X-ray Diffraction. *Chem. Mater.* **2018**, *30*, 6559−6565.

(55) Auras, F.; Ascherl, L.; Hakimioun, A. H.; Margraf, J. T.; Hanusch, F. C.; Reuter, S.; Bessinger, D.; Doblinger, M.; Hettstedt, C.; Karaghiosoff, K.; Herbert, S.; Knochel, P.; Clark, T.; Bein, T. Synchronized Offset Stacking: A Concept for Growing Large-Domain and Highly Crystalline 2D Covalent Organic Frameworks. *J. Am. Chem. Soc.* **2016**, *138*, 16703−16710.

(56) Li, Y.; Guo, L.; Lv, Y.; Zhao, Z.; Ma, Y.; Chen, W.; Xing, G.; Jiang, D.; Chen, L. Polymorphism of 2D Imine Covalent Organic Frameworks. *Angew. Chem., Int. Ed.* **2021**, *60*, 5363−5369.

(57) Lu, X.; Gopalakrishna, T. Y.; Phan, H.; Herng, T. S.; Jiang, Q.; Liu, C.; Li, G.; Ding, J.; Wu, J. Global Aromaticity in Macrocyclic Cyclopenta-Fused Tetraphenanthrenylene Tetraradicaloid and Its Charged Species. *Angew. Chem., Int. Ed.* **2018**, *57*, 13052−13056.

(58) Cheng, Y.-Z.; Ji, W.; Wu, X.; Ding, X.; Liu, X.-F.; Han, B.-H. Persistent radical cation sp^2 carbon-covalent organic framework for photocatalytic oxidative organic transformations. *Appl. Catal. B Environ.* **2022**, *306*, 121110.

(59) Chen, Z.; Li, W.; Sabuj, M. A.; Li, Y.; Zhu, W.; Zeng, M.; Sarap, C. S.; Huda, M. M.; Qiao, X.; Peng, X. Evolution of the electronic structure in open-shell donor-acceptor organic semiconductors. *Nat. Commun.* **2021**, *12*, 5889.

(60) Uribe-Romo, F. J.; Doonan, C. J.; Furukawa, H.; Oisaki, K.; Yaghi, O. M. Crystalline covalent organic frameworks with hydrazone linkages. *J. Am. Chem. Soc.* **2011**, *133*, 11478−11481.

(61) Zeng, Z.; Sung, Y. M.; Bao, N.; Tan, D.; Lee, R.; Zafra, J. L.; Lee, B. S.; Ishida, M.; Ding, J.; Lopez Navarrete, J. T. Stable Tetrabenzo-Chichibabin's hydrocarbons: tunable ground state and unusual transition between their closed-shell and open-shell resonance forms. *J. Am. Chem. Soc.* **2012**, *134*, 14513−14525.

(62) Ni, Y.; Gordillo-Gámez, F.; Peña Alvarez, M.; Nan, Z.; Li, Z.; Wu, S.; Han, Y.; Casado, J.; Wu, J. A Chichibabin's hydrocarbon-based molecular cage: the impact of structural rigidity on dynamics, stability, and electronic properties. *J. Am. Chem. Soc.* **2020**, *142*, 12730−12742.

(63) Su, Y.; Wang, X.; Wang, L.; Zhang, Z.; Wang, X.; Song, Y.; Power, P. P. Thermally controlling the singlet-triplet energy gap of a diradical in the solid state. *Chem. Sci.* **2016**, *7*, 6514−6518.

🕮 Recommended by ACS

Control over Charge Separation by Imine Structural Isomerization in Covalent Organic Frameworks with Implications on CO_2 Photoreduction

Daniel H. Streater, Jier Huang, *et al.*
FEBRUARY 07, 2024
JOURNAL OF THE AMERICAN CHEMICAL SOCIETY   READ 🗗

Structural Conjugation Tuning in Covalent Organic Frameworks Boosts Charge Transfer and Photocatalysis Performances

Qihan Lin, Dan-Wei Zhang, *et al.*
JANUARY 26, 2024
ACS APPLIED MATERIALS & INTERFACES   READ 🗗

Photoenzymatic CO_2 Reduction Dominated by Collaborative Matching of Linkage and Linker in Covalent Organic Frameworks

Qiang Chen, Guangsheng Luo, *et al.*
DECEMBER 18, 2023
JOURNAL OF THE AMERICAN CHEMICAL SOCIETY   READ 🗗

Postsynthetic Annulation of Three-Dimensional Covalent Organic Frameworks for Boosting CO_2 Photoreduction

Pengfei Dong, Jianping Lei, *et al.*
JULY 08, 2023
JOURNAL OF THE AMERICAN CHEMICAL SOCIETY   READ 🗗

Get More Suggestions >